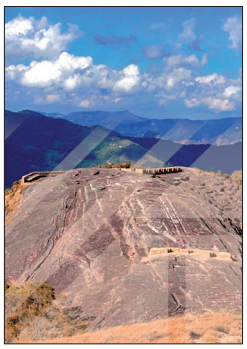

Architectus

2020
2(62)

DOI: 10.37190/arc200211

Anna Kubicka*, Jacek Kościuk**

Determining the rate of erosion and lichen spread on Samaipata rock by comparing 3D laser scan results from two different surveying epochs

Określanie stopnia erozji i tempa rozprzestrzeniania się porostów na skale Samaipata przez porównanie wyników skanowania laserowego 3D z dwóch różnych epok pomiarowych

Introduction

It is becoming increasingly important to preserve and maintain the current condition of cultural heritage sites that have become damaged over the years due to human and natural activity [1]. Proper preservation requires reliable tools that offer accurate diagnostics of current conditions of the site. The latest advances in surveying technology, particularly that of 3D terrestrial laser scanning (TLS), give the opportunity to study damage and material decay using analysis of 3D point clouds generated by different instruments and techniques [2], [3]. Among them, TLS data are widely and successfully used for structural health monitoring in both civil engineering [4] and cultural heritage [5]. This paper focuses on detecting changes to a monument inflicted by climatic erosion, human activity, the spread of lichen, and the progress of archaeological excavations. This monument is El Fuerte de Samaipata – a huge sculptured rock densely covered with petroglyphs, niches, terraces, and platforms. The erosion occurring on Samaipata rock has been addressed by earlier studies [6]–[8] but no attempts to determinate its rate and extent have yet been made.

In the case of Samaipata rock, the main obstacle and difference between similar studies of deformation measurement [9], [10], [2] based on repeated TLS is the considerable disparity in the parameters of the two different instruments used for the scanning – the ILRIS-3D laser scanner produced by Optech in 2006 and the ScanStation P40 introduced by Leica Geosystems in 2016. Both scanners belong to two entirely different epochs of TLS technology development; therefore, their technical characteristics differ considerably.

This paper describes the three issues of 3D scanning the Samaipata rock – the inner registration of the data acquired in two different survey campaigns, the global co-registration of the resulting two 3D point clouds, and the methods of detecting differences between them. Two methods of cloud-to-cloud comparison were used to address the last issue ("nearest neighbour distance" and "local modeling") in CloudCompare – an open source project [11]. In the conclusion of this paper, we will present the potential and limitations of analysing damage on the rock surface using measurements collected by TLS from two different sources.

Acquisition of the TLS data in 2006 and 2016 on El Fuerte de Samaipata

Due to the scale of the entire site – the Samaipata rock itself measures 80 × 240 m and the entire site ca. 400 × 500 m, 3D TLS was the first choice of surveying method. The team from the University of Arkansas collected the

* ORCID: 0000-0001-5442-3947. Faculty of Architecture, Wrocław University of Science and Technology, e-mail: anna.kubicka@pwr.edu.pl

** ORCID: 0000-0003-0623-8071. Faculty of Architecture, Wrocław University of Science and Technology.

first TLS data of the area of sculptured rock in three days (25–27.07.2006) [12]. The instrument used for this purpose, an ILRIS-3D scanner, had a scanning range from 3 to 1200 m, a data acquisition rate of 2000 pts/sec, an angular accuracy of 16″, and a nominal range accuracy of 7 mm@100 m. More details can be found at the manufacturer's website [13]. The area to be scanned was covered with 78 scan stations with an average range accuracy of 20.8 mm@20 m. Particular scans did not cover the full horizontal extent but were limited to 40°/40° angular sections with typical overlap between the scans of not more than 20–30%. This resulted in rather modest density of the final 3D point cloud.

Ten years after the first survey, the team from the Laboratory of 3D Scanning and Modeling covered the area of Samaipata rock with a second TLS survey. In this case, a Leica ScanStation P40 scanner was used. The huge progress in 3D laser scanning technology over the ten years between the first and the last scan resulted in considerable improvement of the technical parameters of scanners. Although the scanning range of the Leica P40 scanner was much shorter (0.4 m to 270 m), for Samaipata rock this had no particular impact. More critical were other parameters – a data acquisition rate reaching 1 mln pts/sec, angular accuracy of 8″ horizontal and vertical, and nominal range accuracy of only 1.2 mm@270 m. More details, particularly on data noise, can be found at the manufacturer's website [14].

Over the 14 days of fieldwork, data from 278 scan stations was collected. Nearly all of the stations covered 360° of horizontal extent, so when all of them were registered into a common coordinate system, the density of the final 3D point cloud was not worse than 5 × 5 mm. Over 14.5 thousand constraints were used for this registration. The mean absolute error for constraints was 3 mm. The most significant errors were noticed on printed black and white (B&W) targets attached to the platforms surrounding the rock, which were caused by heavy vibrations from people walking. Very strong winds also partially affected the small tripods used for the Leica HDS targets. Weighting was used for registration errors not exceeding 10 mm, and in the case of more significant errors, this constraint was eliminated from calculations.

The referencing of all printed B&W targets to the common survey network was done with a Leica TCRP1203 Total Station. Its angular accuracy is of 3″, and the distance error is in the range of ±2 mm + 2 ppm. These parameters, together with angular and distance observations between all pairs of mutually visible positions of the instrument, allowed the survey network points to be aligned with an average x, y point position square error equal to 6.8 mm and average height square error equal to 2.9 mm.

Due to the differences between the technical specifications of both scanners, the scanning parameters, and number of scan stations, point clouds from ILRIS 3D and Leica P40 vary in terms of point density and noise range (Fig. 1).

Global co-registration of the point clouds

The registration of a 3D point cloud from two different surveying epochs and from two different laser scanners was a critical step for the whole procedure. The most popular approach, available in both CloudCompare and Leica Cyclone software is the "Iterative Closest Point" (ICP)

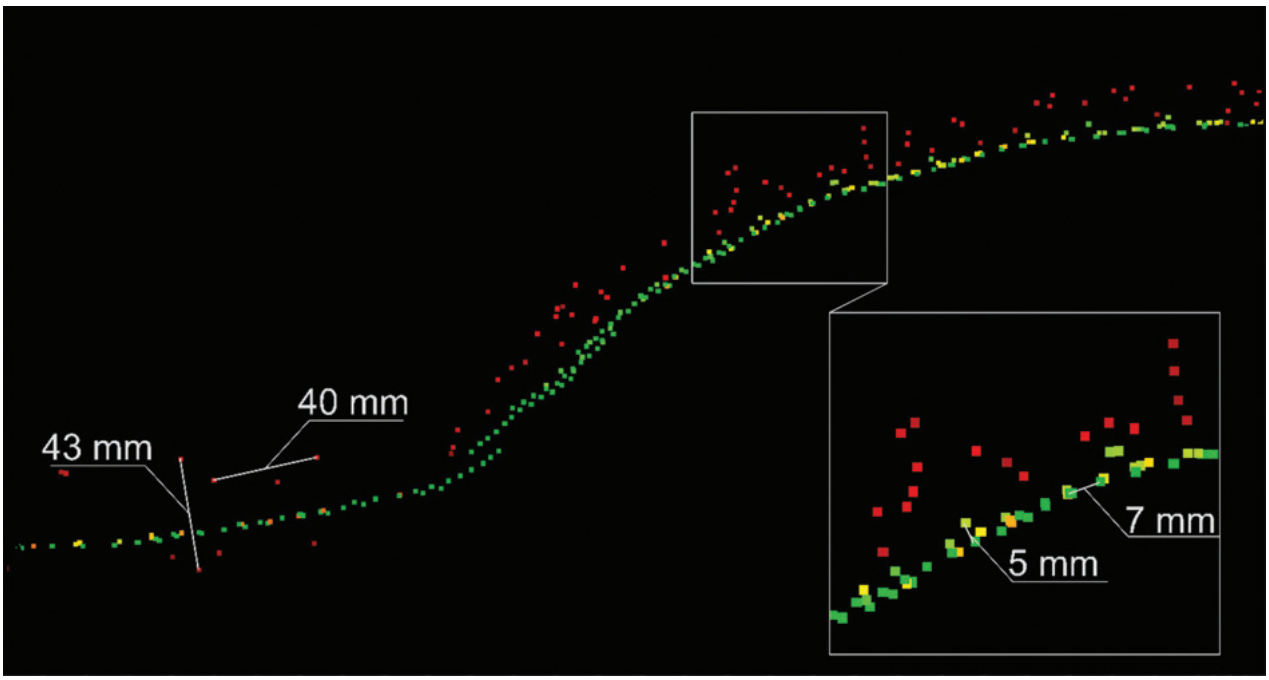

Fig. 1. Section of the point cloud of a petroglyph in sector W05. Visual comparison of point cloud (6 mm width) density and noise range between two 3D point clouds: red – ILRIS 3D (scan 2006); green – Leica P40 (scan 2016) (elaborated by A. Kubicka)

method [15]–[17]. It searches for pairs of nearest points in two data sets and estimates the rigid body transformation that aligns them. This transformation is applied to all points of the transformed data set, and the procedure is repeated until required convergence is achieved [18, p. 5]. Another type of approach used in similar studies for the global 3D cloud as well as the co-registration of surfaces is the method of "Least Squares 3D Surface Matching" (LS3D) [19]. On two overlapping 3D point clouds, this method estimates the transformation parameters of one 3D cloud (or surface) with respect to a 3D template by minimising the sum of squares of the Euclidean distances between the 3D points (or surfaces). Both methods are widely used for the purpose of global co-registration in studies of deformation analyses based on TLS data [9], [10], [20], [21].

The approach proposed in this paper is also based on the ICP method available in Leica Cyclone software for cloud-to-cloud registration. Due to the lack of man-made targets in the 3D point cloud from the 2006 survey, the registration of data from separate scan stations was done by selecting pairs of corresponding points on both 3D clouds. At least four pairs of such points needed to be chosen. Since the density of 3D clouds from the 2006 survey was not very high, it was often difficult to find adequately matching pairs of points, therefore six–eight pairs were usually chosen. In the next step, primary transformation parameters resulting from this rough estimation were further optimised by minimising root mean square (RMS) error. At least 200 iterations were used.

In some cases, due to insufficient overlap between scans from 2006, it was necessary to add scans from the 2016 survey in order to merge all the data into one coherent whole. Since the scans from 2016 were already oriented according to our survey network, choosing one of them as the home scanworld resulted in the same orientation of the entire merged 3D point cloud.

Over 300 constraints were used for this registration. The mean absolute error for constraints was below 5 mm. Weighting was used for registration errors not exceeding 10 mm, and in the case of more significant errors, this constraint was eliminated from calculations.

The final results of co-registering the scans from 2006 and 2016 (Fig. 2) show differences between the extent of these two surveying epochs.

Methods of comparing scan results

In general, results from the two different surveying epochs can be compared in three ways – using only raw data (3D point clouds), using deliverables from processing 3D point clouds (mesh surfaces), or comparing the 3D point clouds to meshes. All of them can be computed with the open source software CloudCompare.

The first method is usually called the *nearest neighbour distance*. This algorithm searches for the Euclidean distance between two nearest points in both the clouds – the reference point cloud and the point cloud being compared [22]. For this method, the denser cloud should be used as the reference point cloud. Only areas exactly covered by both the scans can be directly compared. Otherwise, distorted results can appear.

The second method, known as *global modeling*, compares two surface models (meshes) derived from 3D point clouds. For complicated and detailed surfaces, this involves long computation times. Additionally, local occlusions in compared data resulting in irregular triangular meshing can again lead to erroneous results.

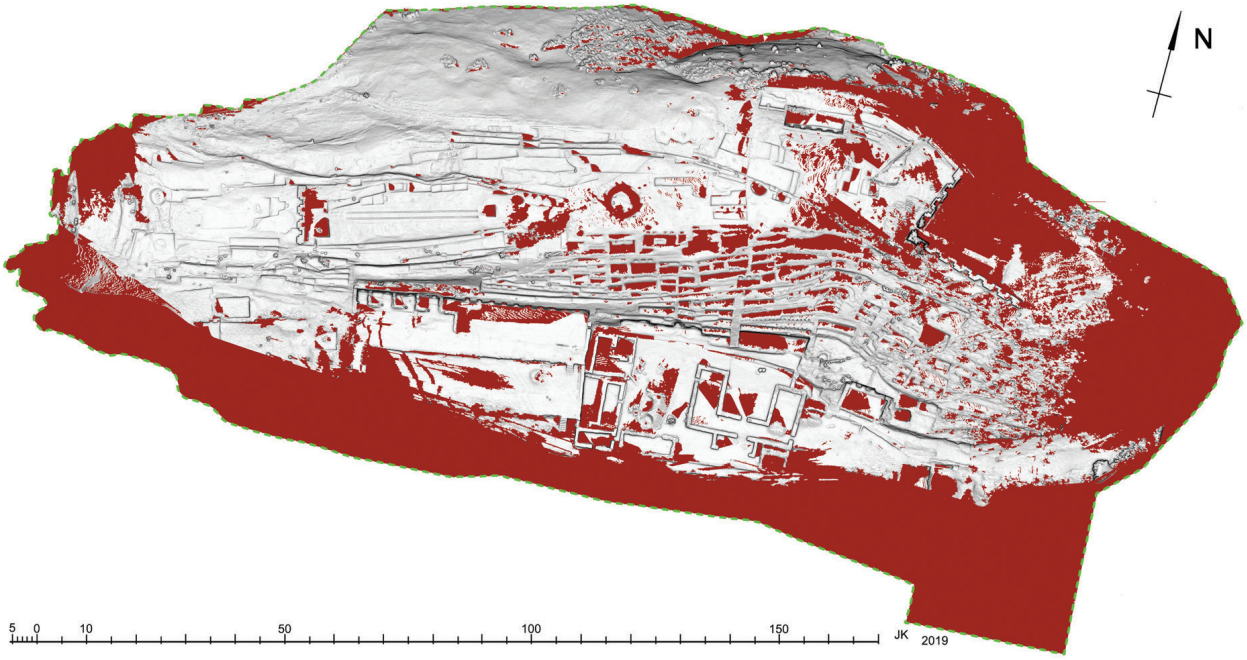

Fig. 2. Comparison of extents of 2006 and 2016 scans.
In grey: areas where both scans overlap, in brown: areas covered by only one scan (either 2006 or 2016)
(elaborated by A. Kubicka)

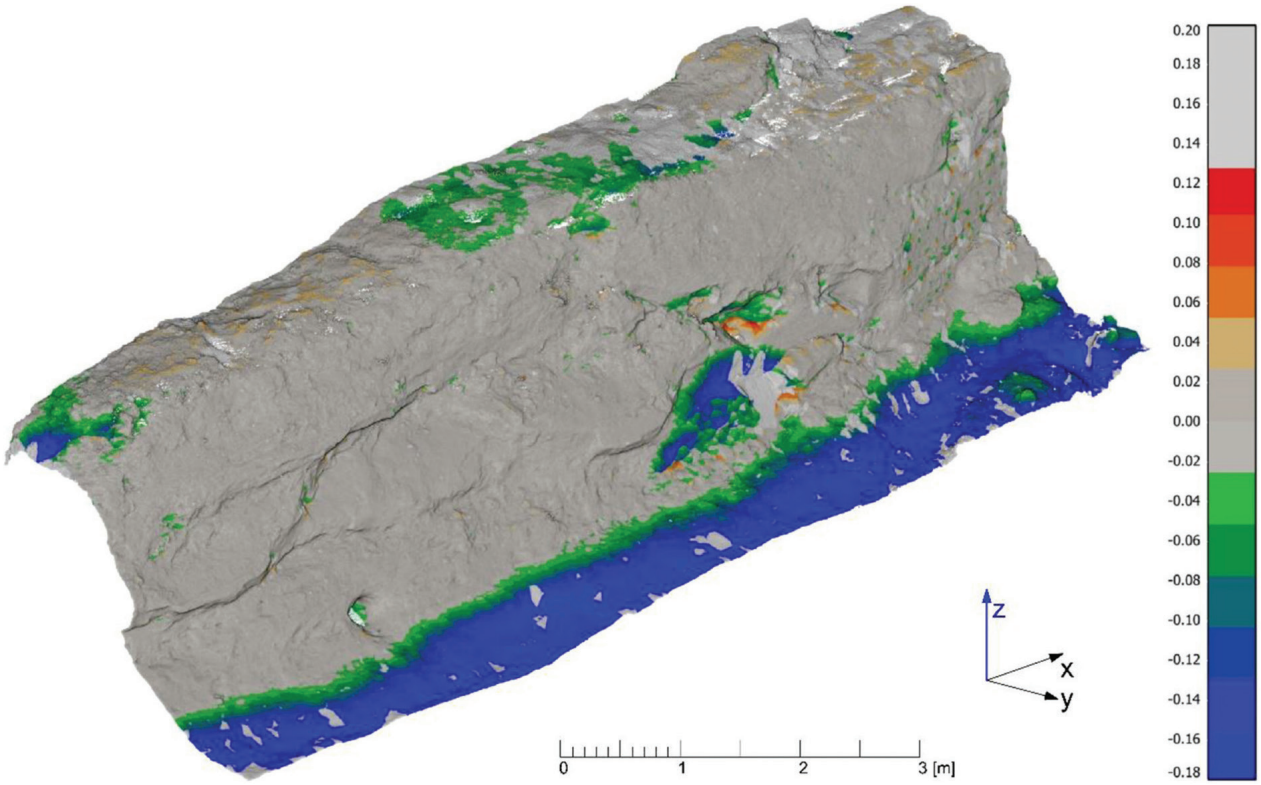

Fig. 3. Part of the front wall of the terrace in sector S27. Results of deformation analysis along the *z*-axis (elaborated by A. Kubicka)

The last method implemented in CloudCompare is called *local modeling*. In this method, the dense 3D cloud is compared to the mesh derived from the sparse point cloud. As a result, the distance is calculated between 3D points on the dense cloud and the nearest point lying on the surface model as a mesh [23]. In addition to reduced computation time, this method also results in better approximation of differences between compared data.

Analysis of changes in the rock surface based on data from two different scanning epochs

Analysis involved three key steps:

– Selecting the specific areas to be analysed. These were typically subsets of the damaged area;

– Orienting the selected area alongside the main axis, so, for example, the vertical face corresponded to the *x*–*z* plane;

– Estimating the deformation parameters for each selected subset.

The smaller the size of the analysed area, the better the resolution of the estimated deformations. Deformations can be analysed alongside specific axes (*x*, *y*, or *z*) or globally. In the last case, the result shows only as absolute values of differences in Euclidean distance, without indicating the dominant direction.

For analysis along one of the selected axes, it is important to consider which of the data sets was the reference data set and which was the compared data set. Therefore, if, for example, the survey from 2016 was mapped as the reference data set, negative values of deformation analysis would correspond to the declined zones of the rock surface, and analogically, positive values would represent material accumulated on the rock surface – mostly, products of rock erosion or vegetation. Reversing the mapping would result in the opposite interpretation.

Due to the high level of noise, especially on scans from 2006, and due to the significant difference in the density of scans from both surveying epochs, a distance of 0.02 m was chosen as the threshold value for detecting deformations. All results below this threshold were treated as a side effect of the technical shortcomings of the scans. In order to eliminate accidental data resulting from inaccurate data filtration (dust particles in the air, people moving through the area, big plants, etc.), the upper threshold for detecting deformations was set to 0.2 m.

As the first example of the feasibility of data sets collected in the year 2006 and 2016 for analysing the progress of erosion on Samaipata rock, the front wall of a terrace in sector S27 will be used[1].

Computation of distances between two data sets analysed alongside the *z*-axis (Fig. 3) showed particularly significant changes (in the range of 0.2 m) at the foot of the vertical wall of the terrace. An analysis of excavation logs indicates that in the years 2006–2016, archaeological works were carried out here. However, the changes within

[1] Cf. J. Kościuk, G. Orefici, M. Ziółkowski, A. Kubicka, R. Muñóz Risolazo, *Description and analysis of El Fuerte de Samaipata in the light of new research, and a proposal of the relative chronology of its main elements*, in the same issue of "Architectus".

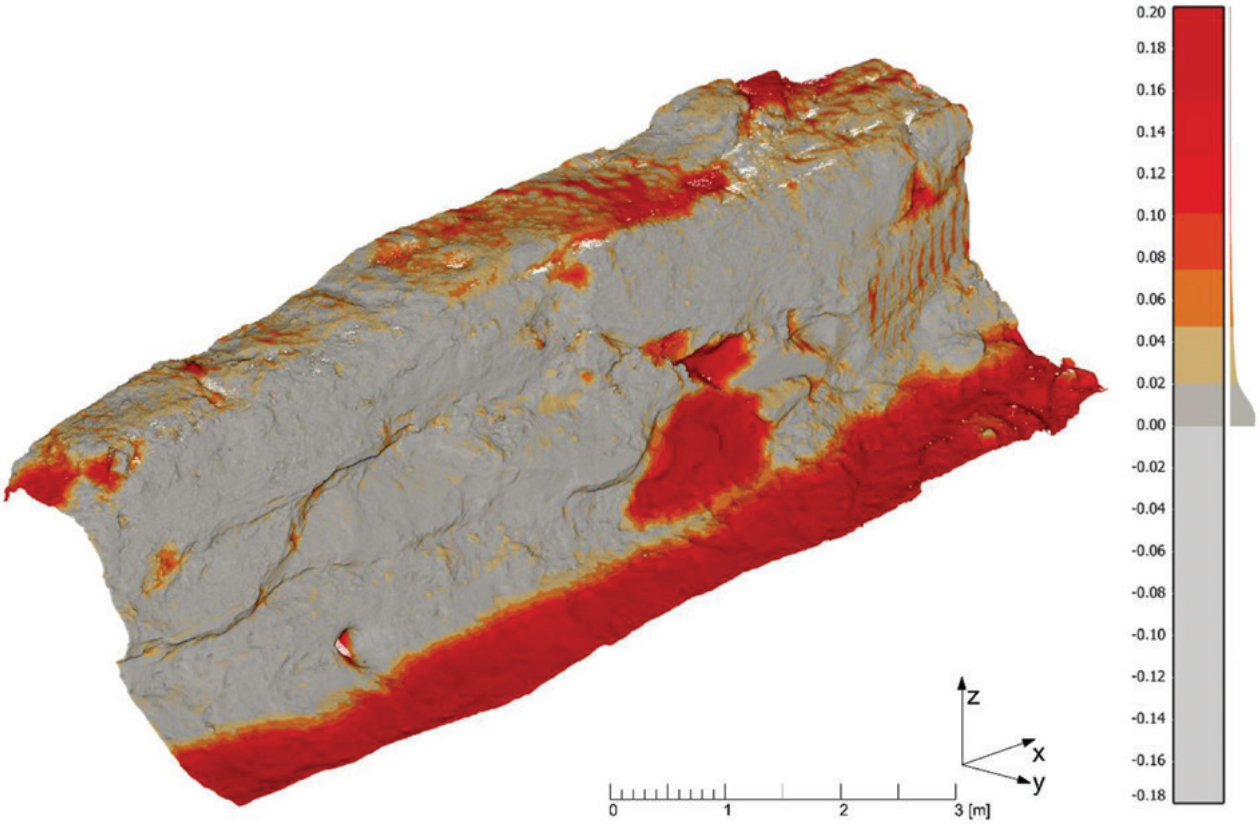

Fig. 4. Part of the front wall of the terrace in sector S27. Results of *global deformation* analysis (absolute values) (elaborated by A. Kubicka)

the terrace front wall cannot be explained by the progress of archaeological prospection. A big cavity, an evident place of local erosion, expanded by more than 0.2 m. Minor changes (0.02–0.06 m) observed in the upper surface of the terrace can be attributed to rock erosion as well as the reduction in vegetation due to the constant efforts of the local restoration team. These observations can be further confirmed by global deformation analysis expressed in absolute values (Fig. 4). In this, the erosion cavities in the front wall are even more visible. Additionally, on the right part of the analysed wall, traces of water erosion (parallel vertical stripes) can be detected.

The highly eroded petroglyph[2] localised in sector W06 can be used as another example of detected rock erosion. In this case, due to much smaller differences, the upper and the lower thresholds were set to ±0.005 m. For this petroglyph, results of *local modeling* along the *z*-axis (Fig. 5) show that mostly the western and northern areas of the petroglyph were influenced by erosion, which ranged from –0.003 m to –0.005 m. The positive values alongside the south-eastern edge of the petroglyph are the effects of growing vegetation.

Analysis of the petroglyph from sector W05 with the clearly recognisable silhouette of a feline is a different case[3]. There, the 3D point cloud acquired in 2006 from the ILRIS 3D scanner has significant noise in the range of ±0.002 m (Fig. 6). Therefore, it was necessary to exclude this range from further interpretations. Expanding the upper and lower thresholds of deformation analysis respectively to –0.010 and +0.06 did not bring particularly useful results. A few positive anomalies (yellow and orange spots) were caused by growing vegetation. Negative anomalies detected in a small ditch encircling the feline figure are the results of erosion caused by water always present in this depression. A more general observation is that the flat areas where rainwater remains for a longer period show positive anomalies (aquamarine colour), while more steep areas present negative anomalies (green colour).

The possible interpretation is that positive anomalies are associated with mosses and lichens that grow better on more wet surfaces, while negative anomalies (on sloping surfaces) are the result of frequent and more rapid changes of moisture in the rock that cause the swelling and shrinkage of smectites present[4]. However, due to the technical

[2] Cf. J. Kościuk, G. Orefici, M. Ziółkowski, A. Kubicka, R. Muñóz Risolazo, *Description and analysis of El Fuerte de Samaipata in the light of new research, and a proposal of the relative chronology of its main elements*, in the same issue of "Architectus".

[3] Cf. J. Kościuk, G. Orefici, M. Ziółkowski, A. Kubicka, R. Muñóz Risolazo, *Description and analysis of El Fuerte de Samaipata in the light of new research, and a proposal of the relative chronology of its main elements*, in the same issue of "Architectus".

[4] Cf. W. Bartz, J. Kościuk, M. Gąsior, T. Dziedzic, *Petrographic, mineralogical, and climatic analyses, and risk maps for conservation strategies*, in the same issue of "Architectus".

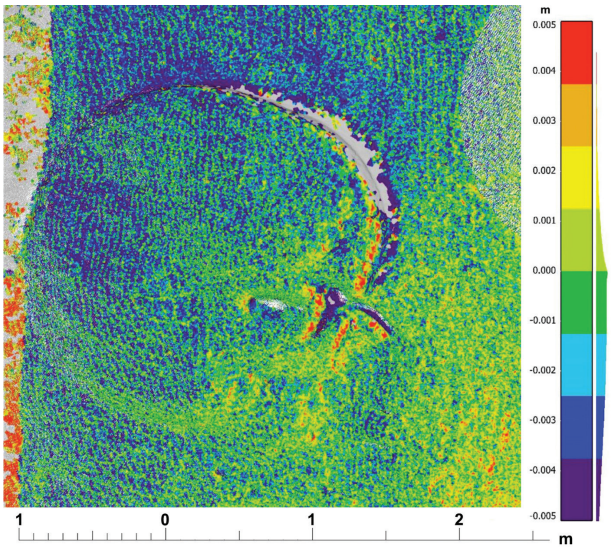

Fig. 5. Petroglyph from sector W06.
Local modeling analysis along the *z*-axis
(elaborated by A. Kubicka)

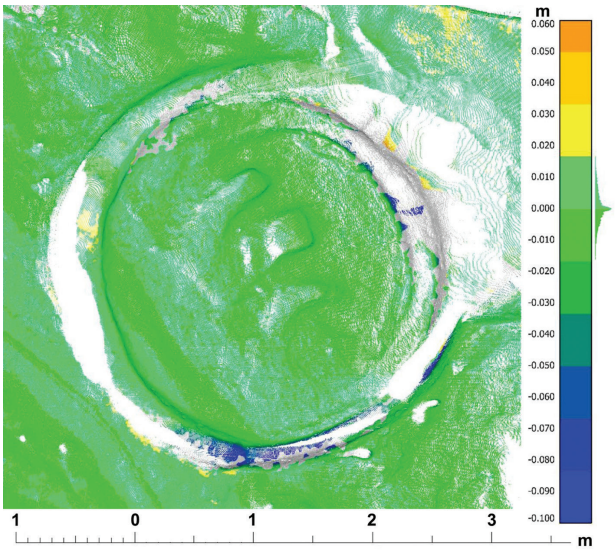

Fig. 6. Petroglyph from sector W05.
Local modeling analysis along the *z*-axis
(elaborated by A. Kubicka)

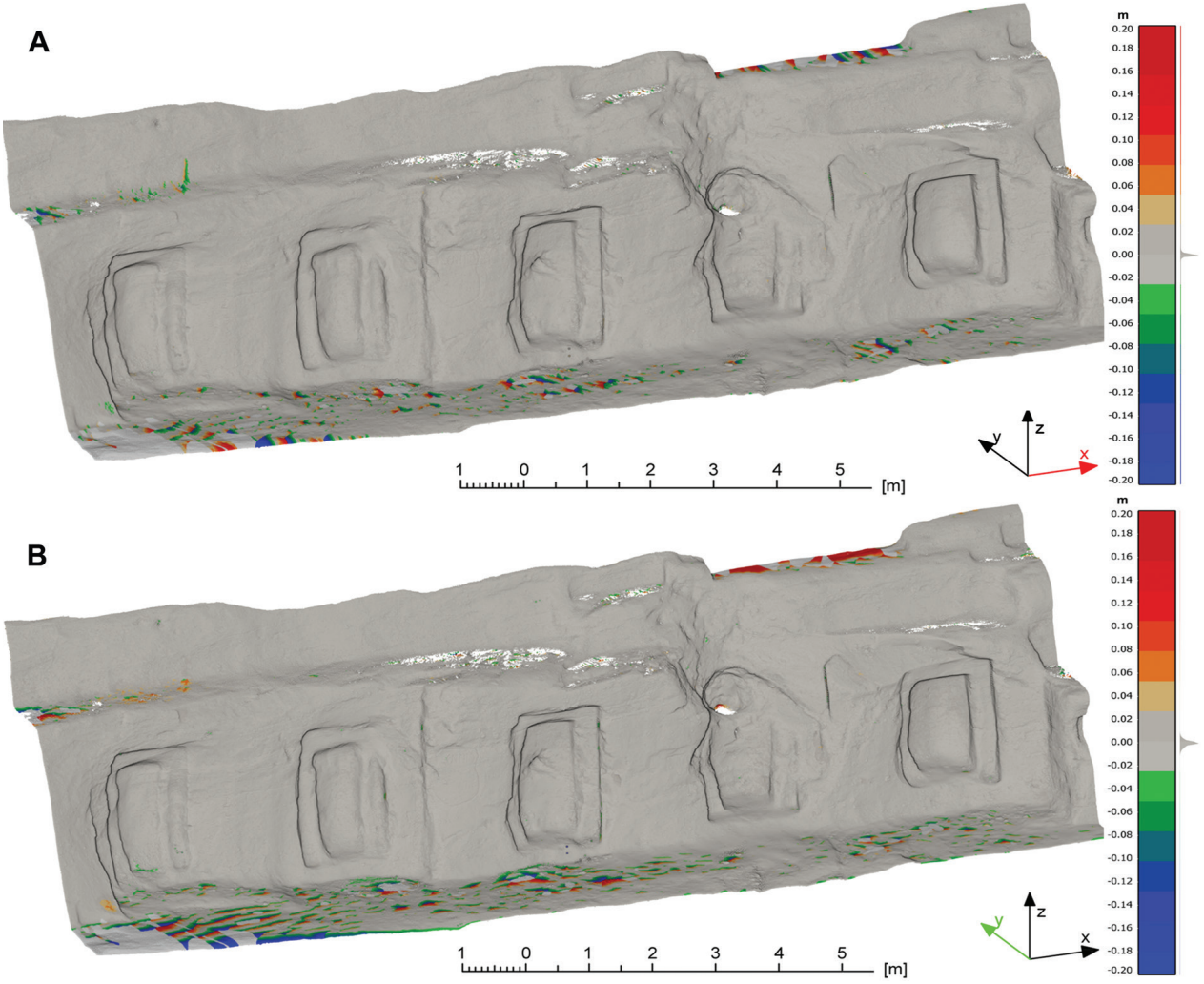

Fig. 7. The southern face of the wall with double recessed niches in sector S09:
A – local modeling analysis along the *x*-axis;
B – local modeling analysis along the *y*-axis
(elaborated by A. Kubicka)

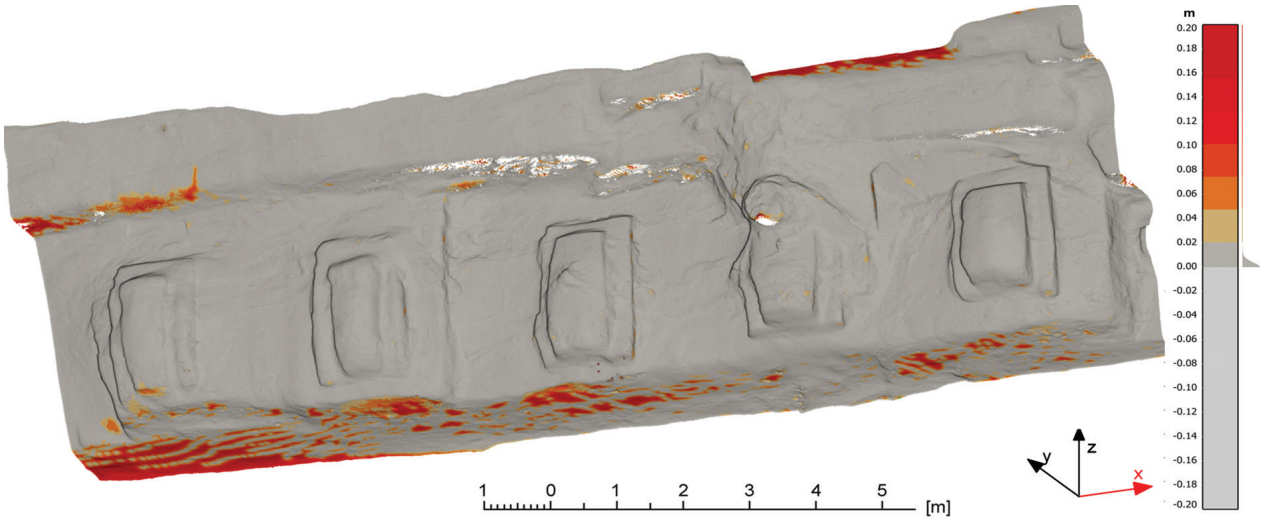

Fig. 8. The southern face of the wall with double recessed niches in sector S09. Global comparison analysis in absolute values (elaborated by A. Kubicka)

Fig. 9. Wall with niches from sector S08. Orthoimage from the 3D point cloud obtained in 2016 with information on lichen spread in 2006 (red colour) and 2016 (green colour) (elaborated by A. Kubicka)

Fig. 10. Wall with double niches from sector S09. Orthoimage from the 3D point cloud obtained in 2016 with information on size of lichens in 2006 (red colour) and 2016 (green colour) (elaborated by A. Kubicka)

shortcomings of the acquired data, all these interpretations should be treated with extreme caution.

In some cases, despite efforts and searching for the best parameters for the analysis, no significant anomalies could be detected. A good example is the unfinished fragment of the southern rock face with double recessed niches lying in sector S09 (Figs. 7, 8). With the upper and lower threshold of deformation analogous to the case of the terrace face in sector S27 (±0.20 m), analysis according to the *x*-axis (Fig. 7A), the *y*-axis (Fig. 7B), and the *z*-axis did not show any noticeable anomalies. The only exception was the flat area in front of the niches where products of erosion (sand and small stones) accumulated. The same results were observed in the *global comparison* analysis (Fig. 8).

Detection and comparison of lichen spread on the surface of the rock

Data from the 2006 and 2016 TLS surveys were also used to detect the spread of lichen. By using different ren-

dering options and different parameters of 3D point cloud visualisation, it was possible to produce natural-colour orthoimages sharp enough to calculate an increase, decrease, or full extinction of lichen. Orthoimages were exported to a CAD 2D environment and then properly scaled and superimposed. The margins of the lichens were then on-screen digitised and areas of each lichen were calculated. Two specific fragments of Samaipata rock were chosen as examples to present the results of this method.

The first example illustrates a case in which lichens identified in 2016 as biologically active using infrared photographs[5] were analysed (Fig. 9). Compared to 2006 data, individual lichens had increased their surfaces by 20–63%. The second example illustrates a case where over the 10 years, some lichens disappeared and new ones started to grow (Fig. 10). Some of them, already invisible in 2006, were able to expand to 0.65 m^2 in 2016.

Again, as in the case of deformation analyses, the quality of scan data played an essential role in the applicability and accuracy of the study. Notably, the density of 3D point data had a direct influence on the quality of resulting orthoimages and therefore on the precision of the margins of lichens on-screen digitising.

[5] Cf. B. Ćmielewski, I. Wilczyńska, C. Patrzałek, J. Kościuk, *Digital close-range photogrammetry of El Fuerte de Samaipata*, in the same issue of "Architectus".

Conclusions: results and limitations

The general conclusion is that despite some technical limitations resulting from the specifications of scanners from two entirely different stages of TLS technology development, the method of monitoring rock erosion and lichen spread by comparing two data sets from two different surveying epochs has great potential. The other factor that should also be taken into account is the fact that the Arkansas team had only three days to complete its fieldwork [12]. The TLS survey in 2016 lasted for 14 days, so the number of overlapping scan stations and resulting density of data was much higher. Nevertheless, despite these limitations, it was possible to detect anomalies in the range of 0.02 m and in some cases even smaller.

Judging from the obtained results, it might be advisable that within the next 10 years, a TLS survey should be repeated with specification (accuracy, density, noise) not worse than that of 2016 – if not a scan of the whole rock, then at least a scan of its most important fragments. Repeated comparison of data from the other two periods will better determine the speed of erosion and indicate the places most exposed to it.

The use of TLS data for monitoring the state of heritage monuments is becoming increasingly common [24], [25] and is particularly worth recommending in the case of El Fuerte de Samaipata.

References/Bibliografia

[1] Moropoulou A., Delegou E.T., Labropoulos K. *et al*., *Non-destructive techniques as a tool for the protection of built cultural heritage*, "Construction and Building Materials" 2013, No. 48, 1222–1239, doi: 10.1016/j.conbuildmat.2013.03.044.

[2] Lachat E., Landes T., Grussenmeyer P., *Comparison of point cloud registration algorithms for better result assessment – towards an open-source solution*, "The International Archives of the Photogrammetry, Remote Sensing and Spatial Information Sciences" 2018, Vol. XLII-2, 551–558, doi: 10.5194/isprs-archives-XLII-2-551-2018.

[3] Rabbani T., Dijkman S., van den Heuvel F. *et al*., *An integrated approach for modelling and global registration of point clouds*, "The International Archives of the Photogrammetry, Remote Sensing and Spatial Information Sciences" 2007, Vol. 61, Iss. 6, 355–370, doi: 10.1016/j.isprsjprs.2006.09.006.

[4] Dąbek P.B., Patrzałek C., Ćmielewski B. *et al*., *The use of terrestrial laser scanning in monitoring and analyses of erosion phenomena in natural and anthropogenically transformed areas*, "Cogent Geoscience" 2018, Vol. 4, No. 1, 1–18, doi: 10.1080/23312041.2018.1437684.

[5] Selbesoglu M.O., Bakirman T., Gokbayrak O., *Deformation Measurement Using Terrestrial Laser Scanner for Cultural Heritage*, "The International Archives of the Photogrammetry, Remote Sensing and Spatial Information Sciences" 2016, Vol. XLII-2/W1, 89–93, doi: 10.5194/isprs-archives-XLII-2-W1-89-2016.

[6] Avilés S., *Conservazione del tempio della rocca scolpita di Samaipata – Santa Cruz, Bolivia (Sudamerica)*, Tesi di Master, Università di Bologna – Sede di Ravenna, Facoltà di Conservazione dei Beni Culturali, Dipartimento di Storie e Metodi per la Conservazione dei Beni Culturali 2002, www.stonewatch.de/media/download/sc%2004.pdf [accessed: 1.11.2019].

[7] Avilés S., *Introduzione alla conservazione della Roccia Scolpita di Samaipata, Bolivia*, 2011, http://www.rupestreweb.info/samaipata.html [accessed: 1.11.2019].

[8] Avilés S., *La conservación de la Roca Sagrada de Samaipata*, [in:] A. Meyers, I. Combès (comp.), *El Fuerte de Samaipata. Estudios arqueológicos*, Universidad Autónoma Gabriel René Moreno, Santa Cruz de la Sierra 2015, 161–170.

[9] Monserrat O., Crosetto M., *Deformation measurement using terrestrial laser scanning data and least squares 3D surface matching*, "The International Archives of the Photogrammetry, Remote Sensing and Spatial Information Sciences" 2008, Vol. 63, Iss. 1, 142–154, doi: 10.1016/j.isprsjprs.2007.07.008.

[10] Gordon S., Lichti D., Stewart M., *Application of a high-resolution, ground-based laser scanner for deformation measurements*, "New Techniques in Monitoring Surveys I, Proceedings of 10th FIG International Symposium on Deformation Measurements" 2001, Orange, California, 23–32, http://webarchiv.ethz.ch/geometh-data/student/eg1/2006/14/HPLAserscanning.pdf [accessed: 20.09.2019].

[11] *CloudCompare open-source software*, http://www.cloudcompare.org/ [accessed: 20.09.2019].

[12] Barnes A., Goodmaster C., Vranich A. *et al*., *The El Fuerte de Samaipata 3D Scanning Project 2005*, http://www.cast.uark.edu/samaipata/index.html [accessed: 20.09.2019].

[13] *ILRIS 3D Datasheet*, https://www.laserscanningeurope.com/sites/default/files/Optech/ILRIS-Datenblatt.pdf [accessed: 20.09.2019].

[14] Leica ScanStation P40/P30, https://leica-geosystems.com/pl-pl/products/laser-scanners/scanners/leica-scanstation-p40--p30 [accessed: 20.09.2019].

[15] Besl P.J., McKay M.D., *A method for registration a 3D shape*, "IEEE Transactions of Pattern Analysis and Machine Intelligence" 1992, Vol. 14, Iss. 2, 239–256, doi: 10.1109/34.121791.

[16] Chen Y., Medioni G.G., *Object Modeling by Registration of Multiple Range Images*, "Proceedings. 1991 IEEE International Conference on Robotics and Automation" 1992, Vol. 10, No. 3, 2724–2729, doi: 10.1109/ROBOT.1991.132043.

[17] Zhang Z., *Iterative point matching for registration of free-form curves and surfaces*, "International Journal of Computer Vision" 1994, Vol. 13, No. 2, 119–152, doi: 10.1007/BF01427149.
[18] Akca D., *Least Squares 3D Surface Matching*, Institut für Geodäsie und Photogrammetrie Eidgenössische Technische Hochschule Zürich, Zurich 2017.
[19] Gruen A., Akca D., *Least Squares 3D Surface and curve Matching*, "The International Archives of the Photogrammetry, Remote Sensing and Spatial Information Sciences" 2005, Vol. 59, Iss. 3, 151–174, doi: 10.1016/j.isprsjprs.2005.02.006.
[20] Barrile V., Meduri G.M., Bilotta G., *Least Squares 3D Algorithm for the Study of Deformations with Terrestrial Laser Scanner*, [in:] V. Mladenov (ed.), *Recent Advances in Electronics, Signal Processing and Communication Systems. Proceedings of the 2013 International Conference on Electronics, Signal Processing and Communication Systems*, Venice, 2013, 162–165, https://www.researchgate.net/publication/280731000_Least_Squares_3D_Algorithm_for_the_Study_of_Deformations_with_Terrestrial_Laser_Scanner [accessed: 1.11.2019].
[21] Monserrat O., Crosetto M., Pucci B., *TLS deformation measurement using ls3d surface and curve matching*, "The International Archives of the Photogrammetry, Remote Sensing and Spatial Information Sciences" 2008, Vol. 37, 591–596, doi: 10.1016/j.isprsjprs.2007.07.008.
[22] Girardeau-Montaut D., Roux M., Marc R. *et al*., *Change detection on point cloud data acquired with a ground laser scanner*, [in:] G. Vosselman, C. Brenner (eds.), *Proceedings of the ISPRS Workshop Laser scanning 2005, ISPRS Archives*, International Institute for Geo-Information Science and Earth Observation, Enschede, 2005, Vol. 36, 30–35, https://www.isprs.org/proceedings/XXXVI/3-W19/papers/030.pdf [accessed: 1.11.2019].
[23] https://www.cloudcompare.org/doc/wiki/index.php? title=Distances_Computation [accessed: 1.11.2019].
[24] Guarnieri A., Milan N., Vettore A., *Monitoring of Complex Structure for Structural Control Using Terrestrial Laser Scanning (TLS) and Photogrammetry*, "International Journal of Architectural Heritage" 2013, Vol. 7, Iss. 1, 54–67, doi: 10.1080/15583058.2011.606595.
[25] Park H.S., Lee H.M., Adeli H. *et al*., *A New Approach for Health Monitoring of Structures: Terrestrial Laser Scanning*, "Computer-Aided Civil and Infrastructure Engineering" 2007, Vol. 22, Iss. 1, 19–30, doi: 10.1111/j.1467-8667.2006.00466.x.

Acknowledgements / Podziękowania

The presented work is part of the research sponsored by the grant given to the Wrocław University of Science and Technology by the Polish National Science Centre (grant No. 2014/15/B/HS2/01108). Additionally, the municipality of Samaipata, represented by Mayor Falvio Lópes Escalera, contributed to this research by providing the accommodation during the fieldwork in June and July 2016, as well as in July 2017. The Ministry of Culture and Tourism of Bolivia kindly granted all necessary permits (UDAM No. 014/2016; UDAM No. 060/2017). The research was conducted in close cooperation with the Centre for Pre-Columbian Studies of the University of Warsaw in Cusco, Peru. Specialists from many other universities and research centres also joined the project. Separate, but no less important, thanks are owed to the University of Arkansas for providing scan data from their survey in 2006.

Abstract

The paper describes the possibility of using 3D laser scans from two different surveying epochs for structural health monitoring. It uses the results of two particular projects – the 2006 3D laser scanning of Samiapata rock by the University of Arkansas and the 2016 3D laser scanning by the Laboratory of 3D Laser Scanning at Wrocław University of Science and Technology – and discusses the methods, results, and limitations of comparing them.

Key words: El Fuerte de Samaipata, Bolivia, terrestrial laser scanning, cloud-to-cloud comparison, structural health monitoring

Streszczenie

W artykule opisano możliwość zastosowania laserowego skanowania 3D z dwóch różnych epok pomiarowych do monitorowania stanu zabytku. Wykorzystano wyniki wykonanego przez University of Arkansas laserowego skanowania El Fuerte de Samaipata z 2006 r. oraz laserowego skanowania 3D z roku 2016 wykonanego przez Laboratorium Skanowania Laserowego 3D Politechniki Wrocławskiej. Omówiono wyniki i ograniczenia proponowanej metody.

Słowa kluczowe: El Fuerte de Samaipata, Boliwia, naziemne skanowanie laserowe, *cloud-to-cloud comparison*, monitorowanie stanu zabytku

Checking data collected of the field
(photo by M. Telesińska)

Sprawdzanie zebranych danych
(fot. M. Telesińska)